JOURNAL OF CATALYSIS 125, 95–111 (1990)

Alkane Rearrangement Pathways on Tellurium-Based Catalysts

ENRIQUE IGLESIA,[1] JOSEPH BAUMGARTNER, GEOFFREY L. PRICE,[2] KENNETH D. ROSE, AND JOHN L. ROBBINS

Corporate Research Science Laboratories, Exxon Research and Engineering Company, Route 22 East, Annandale, New Jersey 08801

Received November 28, 1989; revised March 7, 1990

Isotopic tracer studies and reaction pathway analyses suggest that olefins and diene and triene species are reactive intermediates in *n*-heptane dehydrocyclization on Te/Na*X*. Their concentration is limited by surface hydrogen overpressures caused by a rate-limiting hydrogen desorption step in the dehydrogenation sequence. The distribution of toluene isotopomers formed from dehydrocyclization of *n*-heptane-1-^{13}C is consistent with a reaction sequence involving thermal cyclization of an equilibrated mixture of conjugated and nonconjugated heptatrienes. Methylhexanes are formed predominantly by methyl and ethyl shift reactions of heptenes, and not by hydrogenolysis of C_5 ring species. Alkane hydrogenolysis on Te/Na*X* occurs predominantly by thermal cracking pathways of *n*-heptane and heptenes. No catalytic function for either (1,5) or (1,6) ring closure was observed on Te/Na*X*; a catalytic dehydrogenation function, however, suffices for dehydrocyclization to occur with high selectivity.

1. INTRODUCTION

Alkane dehydrocyclization to aromatic molecules occurs during catalytic reforming of paraffinic naphthas into high octane fuels. Competing isomerization and hydrogenolysis reactions limit dehydrocyclization selectivities. In this study, isotopic tracer and product intercept teachniques, and reaction pathway analyses of *n*-heptane and related probe molecules are used to examine dehydrocyclization, isomerization, and hydrogenolysis pathways on Te/Na*X* catalysts. Specifically, the distribution of toluene isotopomers formed from *n*-heptane-1-^{13}C is used to discriminate among alkane dehydrocyclization models.

The unique properties of Te-loaded zeolites in catalytic alkane dehydrocyclization reactions were first reported by Maile and Weisz (*1*). Several groups have studied the effects of catalyst structure (*2, 3*) and synthesis procedures (*4*) on selectivity, as well as some mechanistic details of the dehydrocyclization step (*5–11*).

2. BACKGROUND

2.1 Dehydrocyclization of Isotopically Labeled Alkanes

The study of toluene isotopomers formed by dehydrocyclization of terminally labeled *n*-heptane is ideally suited to probe the mechanism of alkane ring closure. Several groups have used these techniques in mechanistic studies of alkane dehydrocyclization (*6, 10, 12–22*) and isomerization (*23*) reactions on Pt-, Cr-, and Te-based catalysts. Most studies report label contents in the ring and methyl groups of toluene. Several studies also report detailed label distributions among available ring positions using microwave spectroscopy (*21*) and chemical degradation (*16, 18, 20, 22*) techniques. Here, we report for the first time the ^{13}C NMR determination of toluene isotopomer distributions resulting from *n*-heptane-1-^{13}C dehydrocyclization on Te/Na*X* catalysts.

[1] To whom correspondence should be addressed.

[2] Permanent address: Department of Chemical Engineering, Lousiana State University, Baton Rouge, LA 70803.

0021-9517/90 $3.00

Carbon-13 concentrations at methyl, ortho, meta, para, and at the methyl-bearing (1- or ipso) carbon positions in toluene were measured in order to discriminate among several proposed alkane dehydrocyclization models.

Mitchell (*12*) first reported positionally labeled alkane studies of dehydrocyclization pathways. *n*-Heptane-1-^{14}C dehydrocyclization on Cr_2O_3/Al_2O_3 gave 27% ^{14}C in the methyl group of toluene. *trans*-Annular cyclobutane or cycloheptane intermediates were proposed to explain these results, but later studies suggested that secondary methyl migration and ring hydrogenolysis, catalyzed by residual acid sites, may have influenced their results (*14*). Davis and coworkers (*16, 18*) reported higher label contents in the methyl group (39–43%) and proposed that dehydrocyclization occurred predominantly by (1,6) ring closure on Cr_2O_3/Al_2O_3. However, *n*-heptane-4-^{14}C dehydrocyclization resulted in a measurable carbon-14 content in the methyl group (*16, 18*), suggesting more complex dehydrocyclization pathways, involving (1,7) surface attachment, isomerization, and cyclization without intermediate desorption.

On nonacidic Pt/Al_2O_3, *n*-heptane-1-^{13}C gives toluene with 50% ^{13}C in methyl group, 34% in ortho, and 16% in meta positions (*21*). No label was observed in the para or 1-positions. These authors proposed that dehydrocyclization occurs predominantly by (1,6) ring closure, but also via cyclopentane ring intermediates that undergo selective hydrogenolysis and (1,6) closure without intermediate desorption. At higher alkane conversions, another study reports a lower label content in the methyl group (40–43%) and measurable carbon-14 contents at all ring positions (38.8% ortho, 12.8% para, 3.6% meta, 1.9% 1-position) on Pt/Al_2O_3 (*22*), suggesting secondary dehydrocyclization of methylhexane products. On Te/Na*X*, the ^{14}C content in the toluene methyl group was reported as 50% (*7, 11*).

Recently, several groups have suggested dehydrocyclization mechanisms involving sequential catalytic dehydrogenation of *n*-heptane to *cis*-heptatrienes, followed by thermal (gas-phase) cyclization to methylcyclohexadiene and catalytic dehydrogenation to toluene on Cr (*24*), Pt (*25*), Ni (*25*), and Te (*5, 7, 10*)-based catalysts. Competitive reactions of mixtures of *n*-heptane and labeled heptenes suggest that crossing from Pathway A to B in Scheme 1 (i.e., ring closure) occurs only after the formation of unsaturated intermediates (*24, 25*).

2.2 Alkane Isomerization/Hydrogenolysis Pathways

Alkane isomerization on metals appears to occur by a bond-shift mechanism involving α, α, γ triadsorbed (*26*) or metallacyclobutane (*23*) intermediates (Scheme 2). These mechanisms differ in the rearrangement details and rates as well as in their surface ensemble size requirements and preclude the formation of isomers with quarternary carbons (*27*); these are indeed absent in *n*- and isohexane isomerization on Pt catalysts (*28, 29*).

C_5^+ alkanes, however, can also isomerize via hydrogenolysis of cyclopentane intermediates (*23, 26*), (Scheme 3). Methylcyclopentane hydrogenolysis and *n*-hexane isomerization products on highly dispersed Pt, as well as ^{13}C-distributions in the isomeric products of labeled reactants (*23*), suggest predominantly cyclic pathways on small Pt crystallites. The contribution of bond-shift pathways to alkane isomerization, however, increases as Pt dispersion decreases. On acid sites, alkane isomerization and cracking proceed via carbenium ions that require dehydrogenation of alkane reactants to form gas-phase olefin intermediates (Scheme 3) (*30*).

Thermal cracking of alkanes to lower homologs proceeds at significant rates above ~600K (*31, 32*) and competes effectively with catalytic cracking and hydrogenolysis reactions as reactor temperature increases. Thermal cracking proceeds via noncatalytic β-scission of an equilibrium distribution of heptyl radicals (Scheme 4) (*31, 32*). Primary

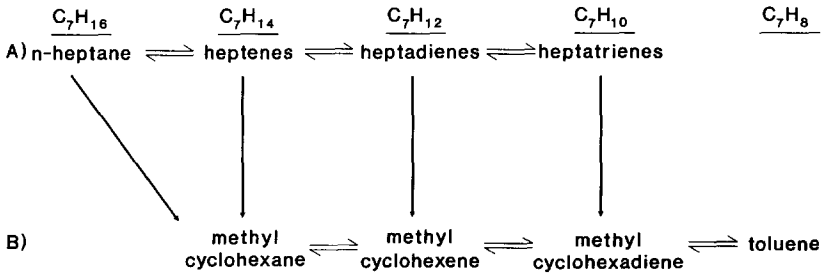

SCHEME 1. *n*-Heptane dehydrocyclization pathways.

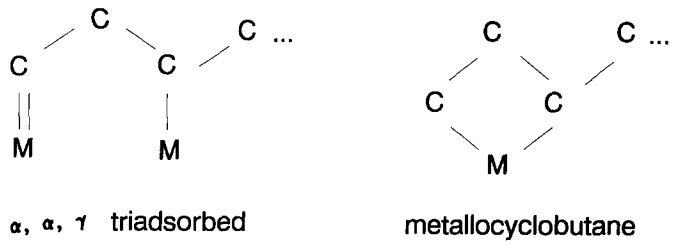

SCHEME 2. Isomerization intermediates on metal surfaces (*23*, *26*).

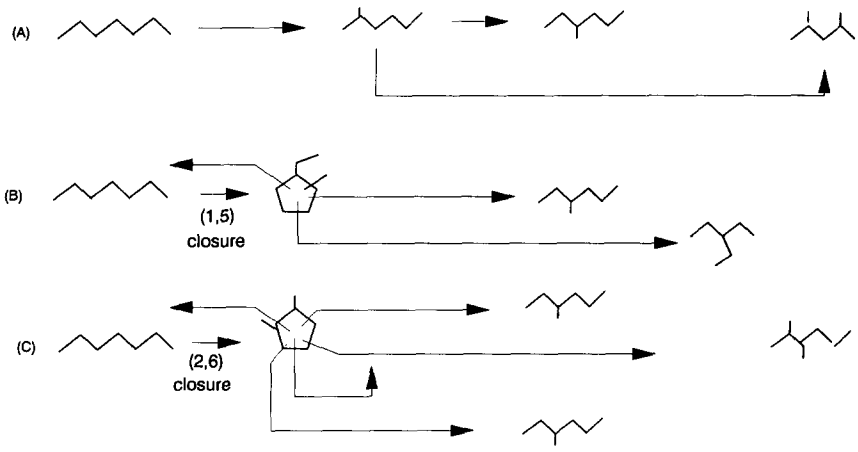

SCHEME 3. *n*-Heptane isomerization pathways. (A) Bond shift; (B and C) cyclic.

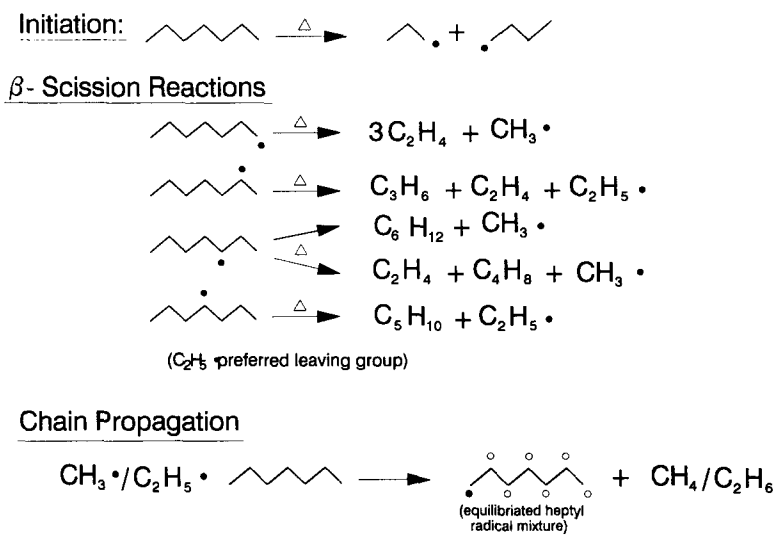

SCHEME 4. *n*-Heptane thermal cracking pathways (*31*).

thermal cracking products show a high olefinic content uncharacteristic of metal-catalyzed alkane hydrogenolysis. *n*-Heptane thermal cracking gives C_2 hydrocarbons with high selectivity, consistent with the stability of C_2-leaving groups in β-scission reactions.

In this study, the role of olefin intermediates and of thermal and acid-catalyzed isomerization and cracking reactions is examined by analysis of contact time effects on product distribution, by the use of product intercept techniques and of 3,3-dimethylpentane isomerization as a sensitive probe of the role of cyclic and bond shift pathways in alkane isomerization.

3. EXPERIMENTAL

3.1. Catalyst Preparation

Tellurium-loaded Na*X* catalysts were prepared by ball milling elemental tellurium with Na*X* zeolite (Linde 13X) for 4 h. The catalyst (10% wt Te before reaction, ~4% wt Te after activation) was activated in flowing hydrogen at 773 K for 4–6 h before catalytic experiments (*1*). The preparation and characterization of Pt-loaded dealuminated Y-zeolite catalysts have been previously described (*33*).

3.2. Synthesis of n-Heptane-1-^{13}C

n-Heptane containing ^{13}C at one terminal carbon position was synthesized by the Cu-catalyzed coupling of *n*-hexylmagnesium bromide with labeled methyl iodide in tetrahydrofuran solvent. The isotopic purity at the terminal *n*-heptane position was greater than 99%. Yields were about 90% compared with 35–65% for the uncatalyzed coupling reaction. Details of the synthesis procedure will be reported elsewhere (*34*).

Unlabeled hydrocarbons were obtained from commercial sources (*n*-heptane, Fluka puriss grade, >99%; heptenes, Aldrich, Gold Label >99%; 3,3-dimethylhexane, Wiley >99%; 3,3-dimethylpentane, Wiley, 99.8%) and degassed by several freeze–thaw cycles.

3.3. Catalytic Measurements

Catalytic reaction studies were carried out in a gradientless glass-recirculating reactor (Fig. 1). Reactants and products were circulated at 100–500 cc(STP)/min using a graphite gear micropump (Micropump, Model 182-336). The system is evacuated using mechanical and diffusion pumps isolated from the system by liquid nitrogen

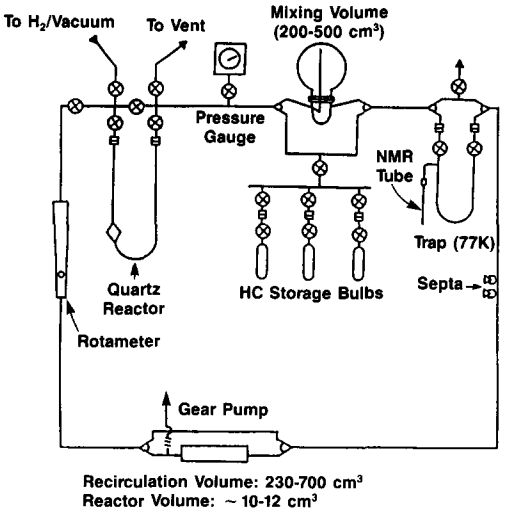

FIG. 1. Schematic diagram of recirculating reactor system.

traps (dynamic pressure, 10^{-4} Pa). In this study, reaction conditions were 673–773 K, 97 kPa dihydrogen pressure, and 4.0–4.5 kPa hydrocarbon pressure. The Te/Na*X* catalyst charge was 0.13 g (~40 μg-atom Te). Dihydrogen (Airco, 99.995%) was purified by passing through a catalytic purifier (Engelhard) and a molecular sieve trap (13X sieve, 77 K).

Products were analyzed using a Hewlett–Packard 5880 gas chromatograph and a Hewlett–Packard 5993A GC/MS. Products were separated by capillary column chromatography (cross-linked methyl silicone, 50 m, 0.32 mm diameter) and their concentrations determined by flame ionization or mass spectrometric detection. Final products were collected at the end of an experiment by trapping them in a cold (~77 K) 5-mm NMR tube containing deuterated chloroform.

Product intercept studies were carried out by generating and collecting in a liquid N_2-cooled trap (77 K) the products (and the unreacted feed) of *n*-heptane reactions on Te/Na*X* (<10% *n*-heptane conversion). These products were then exposed to the Na*X* zeolite or to an empty reactor at reaction conditions in order to determine the role of zeolite-catalyzed and of thermal reactions in product formation.

n-Heptane reaction rates are reported as specific rates [(moles *n*-heptane converted)/(g-cat)-s], metal time yields [(moles *n*-heptane converted)/(g-atom metal)-s], and turnover rates or site–time yields [(moles *n*-heptane converted)/(g-atom surface metal)-s]. Selectivities are reported as the percentage of the converted reactant molecules that appear as a given product. Contact time plots for recirculating batch reactor data are shown as number of turnovers vs. time; their slopes are used to determine turnover rates. Turnovers are defined as the number of moles of reactant (e.g., *n*-heptane) appearing as given product (e.g., toluene) per g-atom Te in the reactor.

3.4. Carbon-13 NMR Measurements

Carbon-13 NMR spectra were obtained on a Varian XL-300 spectrometer operating at 75.42 MHz and on a JEOL GX-400 spectrometer operating at 100.54 MHz. In both cases, gated proton decoupling and a 20-s delay between acquisition pulses were used. Samples were diluted with deuterated chloroform, containing tetramethylsilane as an internal reference, and placed inside a 5-mm NMR tube that tapered to a 1-mm capillary at the end. Chromium acetylacetonate was added in order to ensure complete relaxation of the ^{13}C nuclei between pulses. Integral data for each molecular position were corrected for natural abundance ^{13}C by assuming natural abundance ^{13}C levels at the 3 and 5 positions of the *n*-heptane (methylene resonance at 31.8 ppm) and using the relative concentrations of toluene and *n*-heptane measured by gas chromatography. Resonance assignments were confirmed by means of standard spectral editing sequences (APT and DEPT sequences) that differentiate carbon resonances according to the number of covalently bonded hydrogens.

TABLE 1

n-Heptane Reactions on Te/Na*X* and Pt/Y-Zeolite Catalysts

Catalyst:	Te/Na*X*[a]	Pt/Y-zeolite[b]
Metal time yield (s^{-1}):	3.5×10^{-4}	0.80
Turnover rate (s^{-1}):	3.5×10^{-4}[c]	1.37[c]
n-Heptane conversion (%):	10.6	16.5
Selectivity		
C_1	0.9	1.1
C_2	1.9	0.87
C_3	3.6	1.77
C_4	8.3	2.24
C_5	3.1	2.05
C_6 (aliphatic)	0.9	3.20
C_6 (benzene)	2.6	2.2
Dimethylpentanes	0.1	2.0
2-Methylhexane	5.8	9.2
3-Methylhexane	7.4	14.0
3-Ethylpentane	0.9	2.5
Ethylcyclopentane	0.8	11.4
1,2-dimethylcyclopentane	0.1	1.1
Toluene	34.6	34.7
Olefins, cyclohexadiene, others	Balance	Balance
Cracking to aromatization ratio	0.61	0.39
Isomerization to aromatization ratio	0.40	0.80

[a] 723 K; H_2, 96 kPa;*n*-heptane, 4.5 kPa, 100% Te dispersion.
[b] 673 K; H_2, 96 kPa; *n*-heptane, 4.5 kPa.
[c] Pt dispersion (0.58) by hydrogen chemisorption, Te dispersion (1.00), assumed.

4. RESULTS

4.1. Catalytic Rates and Selectivity

Dehydrocyclization, isomerization, and cracking of *n*-heptane occur simultaneously on Te/Na*X* catalysts (Table 1). Toluene selectivity increases slightly with increasing conversion and contact time because of gradual thermodynamic equilibration of isomerization pathways, but the ratio of dehydrocyclization to cracking (~1.6) remains constant. Cracking occurs preferentially at nonterminal carbons. The carbon number distribution of these cracking products, their high olefin content, and the product intercept studies described later suggest a substantial rate of thermal cracking.

Catalytic rates and selectivities were constant with time and reproducible on several Te/Na*X* catalyst charges. Dehydrocyclization selectivities are very similar on Te/Na*X* and on Pt/Y-zeolite catalysts, but alkane conversion turnover rates are about 4×10^3 lower on Te catalysts (Table 1). *n*-Heptane cracking patterns show a maximum at C_4 on Te/Na*X*, suggesting selective mid-molecule cracking, in contrast with the fairly random carbon–carbon bond cleavage observed on Pt/Y-zeolite catalysts. Alkylcyclopentanes are formed only in small amounts on Te/Na*X* (0.9% selectivity) but are major products and reactive intermediates on Pt catalysts (Table 1).

Toluene, olefin, and *n*-heptane turnovers (n_i) are plotted as a function of contact time in Fig. 2. In a batch recirculating reactor, turnover rates (ν_i) are given by the slope of these curves:

$$\nu_i = \frac{dn_i}{dt}. \tag{1}$$

Toluene turnover plots (Fig. 2c) show an initial zero slope (inflection point), suggesting that toluene formation requires the rate-limiting formation of a reactive intermediate (*B*):

$$A \rightleftarrows B \ldots \rightarrow C$$

$$n\text{-heptane} \rightleftarrows \text{heptenes} \ldots \rightarrow \text{toluene}. \tag{2}$$

Olefin turnover plots (Fig. 2b) suggest that heptenes are reactive dehydrocyclization intermediates; their concentration reaches a steady-state value and then decreases. This behavior is consistent with a sequential reaction scheme that includes heptenes as reactive intermediates; it results from either equilibration of intermediate heptenes with *n*-heptane or from the attainment of a steady-state concentration of such intermediates in a consecutive reaction scheme such as Eq. (2). Heptene/*n*-heptane ratios approach a constant value as contact time increases (Fig. 3). Asymptotic 1-heptene/*n*-heptane ratios are significantly lower than those predicted by thermodynamic calculations (Fig. 3) (*35*). Thus, it would appear that *n*-heptane/heptene equilibration does not occur during dehydrocyclization on Te/Na*X*. However, related studies of *n*-heptane–deuterium exchange and isotopic carbon equilibration suggest that thermody-

namic equilibrium is achieved under reaction conditions but that it occurs at a surface with a substantial hydrogen virtual pressure (*34*); this surface overpressure is caused by the rate-limiting desorption of hydrogen from the surface during the catalytic dehydrogenation step. In any case, heptenes appear to be reactive intermediates for at least some *n*-heptane conversion pathways on Te/Na*X*.

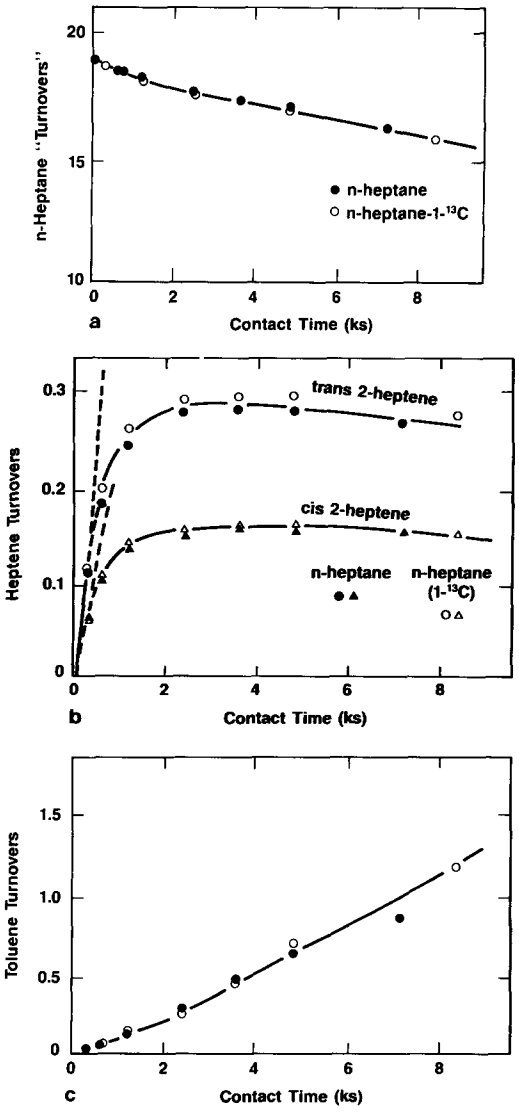

FIG. 2. *n*-Heptane reactions on Te/Na*X* (batch recirculating reactor; 723 K; *n*-heptane,4.5 kPa; hydrogen, 96 kPa). (a) *n*-Heptane, (b) olefins, (c) toluene.

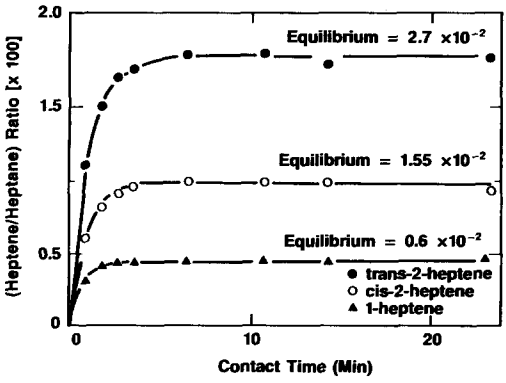

FIG. 3. Heptene to *n*-heptane ratios on Te/Na*X* (723 K; *n*-heptane, 4.5 kPa; hydrogen, 96 kPa).

4.2. Dehydrocyclization of n-Heptane-1-^{13}C

Labeled (1-^{13}C) and unlabeled *n*-heptane reactants gave similar conversion rates and heptene and toluene selectivities (Fig. 2). Isotopomer distributions were measured by ^{13}C NMR analysis of reaction products collected after 3.6 ks (7.2% *n*-heptane conversion) and 22.7 ks (33.9% *n*-heptane conversion) contact times. Isotopomer distributions corrected for natural abundance of ^{13}C (1.1%) are shown in Table 2.

Carbon-13 appears predominantly in the methyl and ortho positions within toluene molecules. Isotopomer distributions are independent of contact time except for a slight increase in ^{13}C enrichment in the meta and ipso positions at longer contact times. Therefore, the observed distribution arises from primary *n*-heptane-1-^{13}C dehydrocyclization pathways, rather than from secondary reactions, such as (1,6) ring closure of methylhexanes or methyl migration (isotopomerization) within toluene molecules. The ring ^{13}C content is slightly above 50% (~52%) and also independent of contact time. ^{13}C enrichment occurs only at methyl groups in 3-methylhexane, 2-methylhexane, and ethylpentane molecules (Table 2).

A typical ^{13}C NMR spectrum of a toluene product derived from *n*-heptane-1-^{13}C is shown in Fig. 4. Five resonances are as-

TABLE 2

^{13}C Distribution *n*-Heptane-1-^{13}C Reaction Products (Te/Na*X*)[a]

Contact time (ks):	3.6	22.7
n-Heptane conversion (%):	7.2	33.9
^{13}C distribution (%)		
Toluene		
Methyl-	48.1	47.7
Ortho-	47	46.0
Para-	1.1	1.0
Meta-	3.8	4.6
1-	0	0.6
3-Methylhexane		
CH_3 (1,6,7) positions	—	100
CH_2, CH (2,3,4,5)	—	0
3-Ethylpentane		
CH_3 (1,5,7)	—	100
CH_2, CH (2,3,4,6)	—	0
2-Methylhexane		
CH_3 (1,6,7)	—	100
CH_2, CH (2,3,4,5)	—	0

[a] From NMR measurements.

signed as indicated in the figure caption to the nonequivalent carbon positions in the toluene molecule. The vertical adjustments in this figure are identical for the aromatic and methyl resonances. A sixth resonance appearing at 128.4 ppm in this spectrum is due to benzene, a product of the catalytic reaction that was independently identified by gas chromatography.

In unenriched toluene molecules, the intensity of each resonance is proportional to the number of carbons in each unique carbon environment within toluene. For example, two resonances—those at 128.5 and 129.2 ppm—normally appear with twice the intensity of those at other toluene positions. Figure 4 shows that the methyl and ortho carbons in the toluene product are more isotopically enriched than the ipso, meta, and para carbons.

4.3 Dehydrocyclization of 1-Heptene/n-Heptane-1-^{13}C Mixtures

The role of olefin intermediates in *n*-heptane dehydrocyclization was examined by measuring the relative rates of isotopic

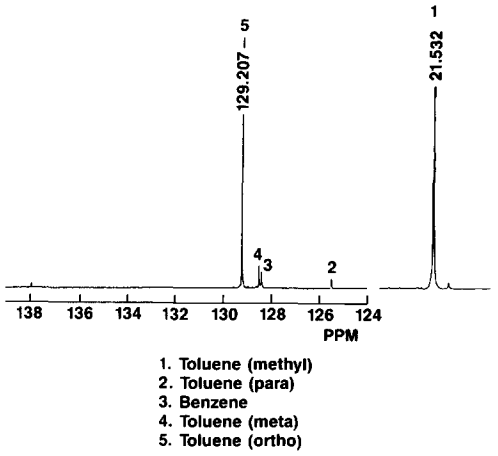

FIG. 4. Carbon-13 NMR spectrum of *n*-heptane-1-^{13}C dehydrocyclization products (toluene region).

transfer from a 1-heptene (20%)/*n*-heptane-1-^{13}C (80%) mixture into the toluene, isoalkanes, and internal olefin products. The ^{13}C content of reactants and products was measured by mass spectrometry after capillary chromatographic separation; it is plotted as a function of contact time in Fig. 5.

^{13}C equilibrates between heptenes and *n*-heptane in about 2 ks. Before equilibration, however, ^{13}C concentrations in olefins and toluene are similar both in trend and in absolute value. These data demonstrate that tol-

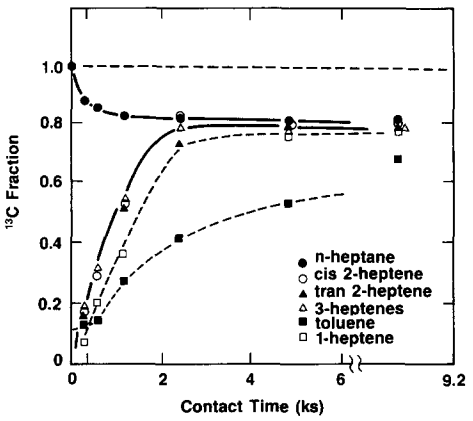

FIG. 5. ^{13}C fraction in reaction products from 1-heptene (20%)/*n*-heptane-1-^{13}C (80%) mixtures (723 K; hydrocarbons, 4.5 kPa; hydrogen, 96 kPa).

uene is predominantly and preferentially formed via heptene intermediates that are apparently required for *n*-heptane dehydrocyclization on Te/Na*X*. Moreover, *n*-heptane dehydrogenation and heptene hydrogenation processes are slow ($\tau \sim 2$ ks) but equilibration among heptenes (double-bond isomerization) occurs rapidly ($\tau < 0.3$ ks). The constant ratio of heptene to heptane concentrations and their identical isotopic composition (after 2.0 ks) demonstrates the establishment of hydrogenation–dehydrogenation equilibrium. However, as discussed previously, observed olefin concentrations are below their predicted thermodynamic values. Rate-limiting hydrogen desorption and the resulting hydrogen surface overpressures are apparently responsible for these differences. The details of this model, as well as supporting hydrocarbon–D_2 exchange and kinetic studies, are described in detail elsewhere (*36*).

The ^{13}C content in toluene remains lower than those of other products (and reactants) even after long contact times, even though the entire reactant pool (*n*-heptane, heptenes) is isotopically equilibrated at a higher ^{13}C content (76–81%) after about 2 ks (Fig. 5). This is the result of the high reactivity and zero initial ^{13}C content of 1-heptene compared to those of *n*-heptane-1-^{13}C, which leads to a very high concentration of ^{12}C in the initial toluene product. Toluene does not reequilibrate with the reactant pool because of the presence of at least one irreversible elementary step in the heptene dehydrogenation/cyclization sequence.

The molar concentrations of labeled and unlabeled toluene are shown in Fig. 6 as a function of contact time. The zero initial slope for the ^{13}C-toluene concentration curve shows that toluene formation proceeds predominantly via intermediate conversion of *n*-heptane-1-^{13}C to heptenes. The unlabeled toluene concentration curve, however, shows a sharp initial increase, suggesting a fast rate of formation from the unlabeled heptenes. After *n*-heptane–heptene isotopic equilibriation ($\tau > 2$ ks), the

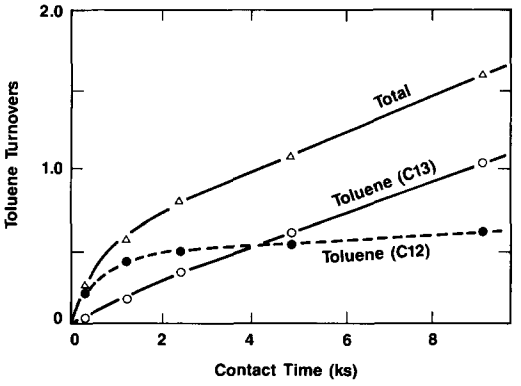

FIG. 6. Moles of labeled and unlabeled toluene formed from 1-heptene (20%)/*n*-heptane-1-^{13}C (80% mixtures) (723 K; hydrocarbon, 4.5 kPa; hydrogen, 96 kPa).

slopes of the labeled and unlabeled toluene curves merely reflect the relative isotopic content of the equilibrated reactant pool. The initial slopes in Fig. 6 show that the rate of heptene dehydrocylization is at least 50 times faster than that of *n*-heptane (for 80/20 initial mixtures); therefore, heptenes are *reactive* intermediates in *n*-heptane dehydrocyclization. The apparent zero slope in the labeled toluene curves suggests that no direct alkane dehydrocyclization pathways exist on Te/Na*X*.

4.4 Dehydrocyclization of n-Heptane/Toluene-methyl-^{13}C Mixtures

The reversibility of the alkene cyclization (ring closure) step was examined by measuring the isotopic scrambling of ^{13}C in toluene-methyl-^{13}C and the appearance of labeled *n*-heptane and heptenes during dehydrocyclization on Te/Na*X*. The ^{13}C NMR analysis of the resulting product is shown in Table 3. After 15 ks (~25% *n*-heptane conversion), less than 0.5% of the ^{13}C label was incorporated into the toluene ring (Table 3) and less than 0.3% appeared in *n*-heptane and heptenes; it appeared exclusively at the ortho position in toluene and at the terminal carbon in *n*-heptane. Therefore, one or more steps in the catalytic formation of toluene are irreversible, and secondary toluene or *n*-

TABLE 3

^{13}C Distribution in *n*-Heptane/Toluene (^{13}C-*methyl*) Reaction Products

	% ^{13}C enrichment[a]	
	Initial	Final
Toluene		
Methyl	100	99.5
Ortho	0	~0.5
Para	0	0
Meta	0	0
1-Position	0	0
n-Heptane		
1 or 7	0	<0.3
2 or 6	0	0
3 or 5	0	0
4	0	0

[a] Corrected for natural abundance of ^{13}C [723 K; 13% toluene (^{13}C-*methyl*); 87% *n*-heptane; 96 kPa hydrogen; 4.5 kPa hydrocarbons; after 16 ks; 26% *n*-heptane conversion].

heptane isotopomerization reactions do not scramble methyl carbons into the ring structure or into internal carbon positions in *n*-heptane. Thus, these reactions cannot be responsible for the ^{13}C enrichment in meta and para positions observed during *n*-heptane-1-^{13}C dehydrocyclization.

4.5 Product Intercept Studies

Zeolite-catalyzed and thermal reactions of the products of *n*-heptane rearrangements on Te/Na*X* were examined by collecting such products in a cold trap (77 K) after about ~10% *n*-heptane conversion, and subsequently allowing them to contact at reaction conditions (723 K, 96 kPa H_2) a Na*X* sample or an empty reactor.

Toluene formation stops immediately when Te/Na*X* is replaced with Na*X* or with a blank reactor (Fig. 7a). Isomerization continues over Na*X* but at much lower rate, suggesting that olefins do not undergo significant acid-catalyzed isomerization on neat Na*X* (Fig. 7b); either such a Na*X*-catalyzed reaction requires highly unsaturated

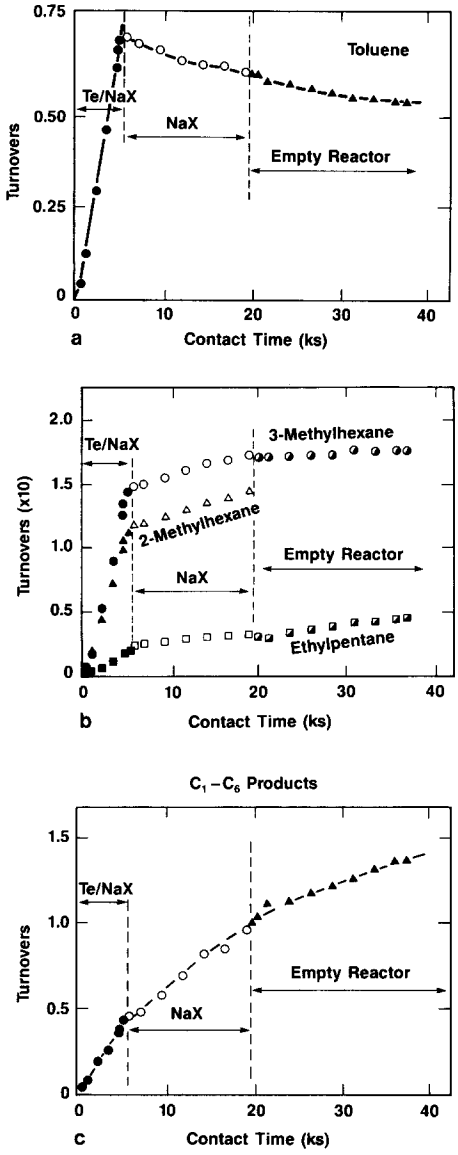

FIG. 7. Product intercept studies. Turnovers vs contact time for (a) toluene, (b) isoalkanes, (c) C_1–C_6 products (723 K; *n*-heptane, 4.5 kPa; hydrogen, 96 kPa).

intermediates that are quickly consumed and not being replaced by dehydrogenation reactions normally occurring on Te sites, or coupled Te–Na*X* sites are required for heptene isomerization. Isomerization does not occur in an empty reactor (Fig. 7b).

The total cracking rate (C_1–C_6 products)

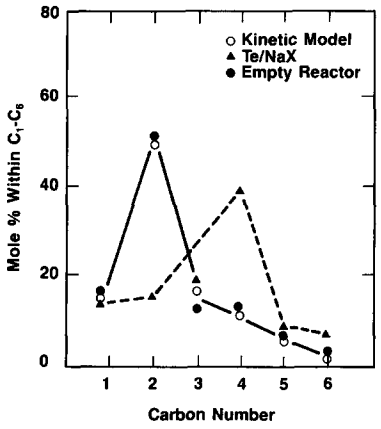

FIG. 8. C_1–C_6 product distributions. Comparison of Te/Na*X*, empty reactor, and kinetic model (723 K; *n*-heptane, 4.5 kPa; hydrogen, 96 kPa).

is not strongly affected by replacing Te/Na*X* with Na*X* or a blank reactor except for the expected decrease in rate as the more reactive olefins are consumed (Fig. 7c). The *n*-heptane cracking patterns obtained on TeNa*X* and in a blank reactor are compared in Fig. 8. A distinct shift toward higher molecular weight products, especially C_4, on Te/Na*X* and the formation of higher molar amounts of C_6, C_5, and C_4 compared with their coproducts C_1, C_2, and C_3, respectively, suggest that secondary coupling reactions occur on the catalyst following thermal cracking. C_2–C_6 products are highly olefinic, consistent with a significant contribution of thermal cracking pathways. A decrease in the rate of C_4 formation and a marked increase in the rate of formation of C_2 products occurs in product intercept studies when Te/Na*X* is replaced with Na*X* or an empty reactor, suggesting the presence of an ethylene dimerization functionality on Te/Na*X*. Ethylene cofeed experiments also showed that Te-catalyzed secondary dimerization of olefinic thermal cracking products occurs; this secondary reaction of primary cracking products accounts for the observed changes in cracking selectivity, but not rates, in the presence of Te/Na*X*.

4.6 3,3-Dimethylpentane Isomerization

Contact time effects on the isomerization products of *n*-heptane and 3,3-dimethylpentane reactions were used to determine the relative contribution of C_5-ring hydrogenolysis and of carbenium ion/bond-shift pathways to isomerization reactions on Te/Na*X*. Scheme 5 shows that 2,2-dimethylpentane and 2,3-dimethylpentane are primary products of the isomerization of 3,3-dimethylpentane via C_5-ring and bond-shift pathways, respectively. Both products are observed on Te/Na*X* (Fig. 9a); their initial rate of formation is small, suggesting that like toluene they require the initial buildup of olefin intermediates. Extrapolation of the concentrations of these two product isomers to zero contact time (Fig. 9b) gives:

$$\frac{[\text{2,2-dimethylpentane}]}{[\text{2,3-dimethylpentane}]} = 0.04,$$

suggesting that bond-shift pathways are predominantly responsible for the observed isomerization products. Increasing contact time leads to secondary isomerization of these primary products via sequential bond-shift-type reactions.

Ring closure of 3,3-dimethylpentane on Te/Na*X* is very slow and the resulting C_5-ring intermediates do not undergo significant hydrogenolysis (to methylhexanes) or ring enlargement (to methylcyclohexane/toluene).

5. DISCUSSION

5.1 Dehydrocyclization Pathways on Te/NaX Catalysts

Contact time effects on toluene and heptene turnovers and the initial selective formation of ^{12}C-toluene from 1-heptene/*n*-heptane-1-^{13}C mixtures suggest that olefins are reactive intermediates in *n*-heptane dehydrocyclization. These data suggest that *n*-heptane dehydrogenation to heptenes is a required step in the overall catalytic sequence. Double-bond isomerization of heptene is rapid and is near thermodynamic and

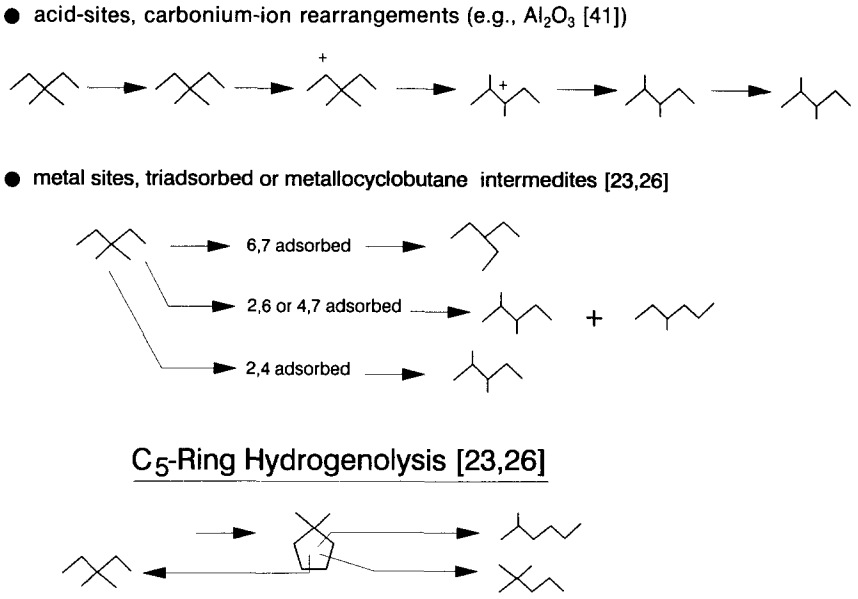

SCHEME 5. Cyclic and bond-shift rearrangements of 3,3-dimethylpentane.

isotopic equilibrium under reaction conditions (Fig. 5). Olefin/paraffin equilibration occurs after the initial stages of the reaction, but "equilibrium" olefin concentrations are limited by a rate-controlling hydrogen desorption step that leads to hydrogen surface overpressures (*36*) and to olefin contents lower than thermodynamic predictions.

Our data suggest that the crossover cyclization step between Pathways A and B in Scheme 1 is thermal; it occurs after initial dehydrogenation of *n*-heptane and most

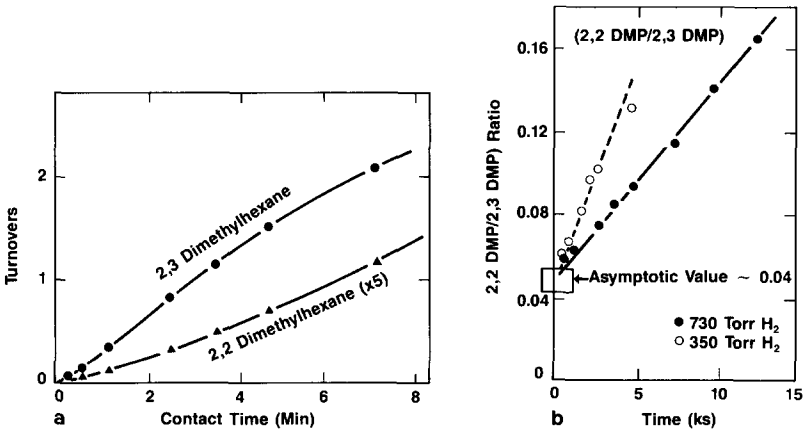

FIG. 9. 3,3-Dimethylpentane isomerization on Te/Na*X*; (a) isoalkane turnovers vs contact time; (b) 2,2-dimethylpentane to 2,3-dimethylpentane product ratio (723 K; 3,3 dimethylpentane, 4.5 kPa; hydrogen, 96 kPa).

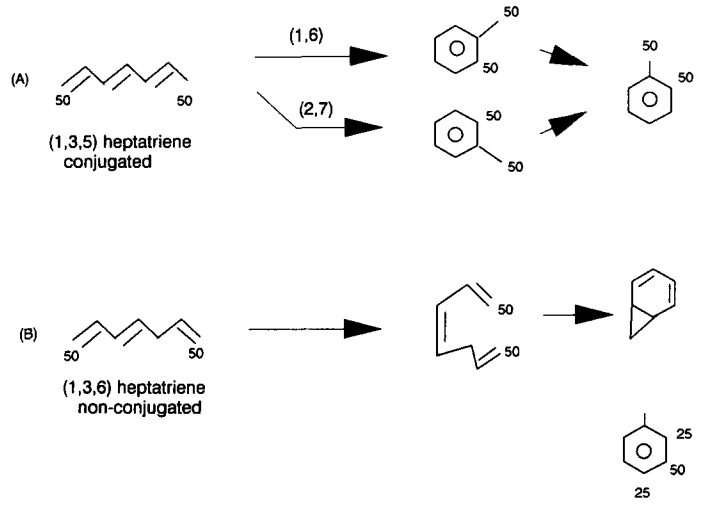

SCHEME 6. Electrocyclic addition reactions of conjugated and unconjugated heptatrienes.

likely after subsequent dehydrogenation to heptadiene and heptatriene species. Heptatrienes are known to cyclize rapidly to methylcyclohexadienes via intramolecular Diels–Alder reactions (*37, 38*). They have been previously proposed as reactive intermediates in alkane dehydrocyclization on Te/Na*X* (*5, 7, 10*) and other catalysts (*24, 25*). As shown below, the isotopomer distribution in toluene formed from terminally labeled *n*-heptane is also consistent with the thermal cyclization of heptatriene species.

Direct (1,6) or (2,7) closure of terminally labeled heptatriene species leads exclusively to ^{13}C enrichment at the methyl and ortho positions; it cannot account for the experimental meta (3.8–4.6%) and para (1.0–1.1%) ^{13}C enrichments (Table 2). Bicyclo species formed by cyclization of nonconjugated heptatrienes, however, can account for primary meta and para enrichment (Scheme 6). Thermal cyclization of nonconjugated trienes formed from *n*-heptane-1-^{13}C lead to ^{13}C enrichment at ortho (25%), meta (50%), and para (25%) positions. Scheme 6 describes how such reactions provide pathways for meta- and para-^{13}C enrichment in toluene. Allenic triene species are not included in Scheme 6 because of their high free energies of formation.

The rapid isomerization of heptenes on Te/Na*X* (Fig. 4) suggests that double-bond migration proceeds much more rapidly than heptene hydrogenation and dehydrocyclization or *n*-heptane dehydrogenation. Therefore, thermodynamic equilibrium between very reactive conjugated and nonconjugated *cis*-heptatrienes is also likely to occur rapidly on Te/Na*X*; the relative equilibrium concentrations of conjugated and nonconjugated heptatrienes would then determine the relative contributions of Pathways A and B in Scheme 6, and thus the isotopomer distribution in toluene, provided that:

(i) triene cyclization rates are similar in Pathways A and B and,

(ii) cyclopropane rings open with equal probability at both available carbon–carbon bonds.

Free energes of formation of heptatriene isomers were not found in the literature. Therefore, the equilibrium concentrations of these isomers were estimated from available free energy data for conjugated and nonconjugated pentadienes (*35*):

(a) *cis*-1,3 pentadiene 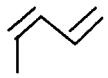

$\Delta G° = 18.9$ kJ/mol

(b) 1,4-pentadiene 

$\Delta G° = 17.2$ kJ/mol

(c) trans-1,3 pentadiene 

Heptatrienes with a *cis* configuration at the 3-position are needed to achieve the molecular orbital overlap required for the electrocyclic addition reaction to occur (*39*). These *cis*-3 isomers are:

(d) 1, *cis*-3, *cis*-5-heptatriene 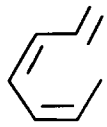

$\Delta G° = 18.9$ kJ/mol

(e) 1, *cis*-3, 6-heptatriene 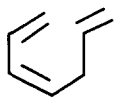

$\Delta G° = 17.2$ kJ/mol

(f) 1, *cis*-3, trans-5-heptatriene 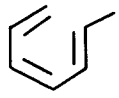 ,

where free energy differences are estimated by analogy with pentadiene data. Species (e) and (f) can cyclize by the electrocyclic addition reactions described in Scheme 6. Species (d), however, requires a highly unstable rotational conformation or isomerization to more stable structures (e.g., (e) or (f)) for orbital overlap to occur (d_2):

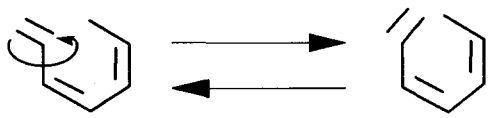

(d_1) (d_2)

TABLE 4

Comparison of Observed and Calculated ^{13}C Distributions in Toluene (*n*-Heptane-1-^{13}C, Te/Na*X*)

	% ^{13}C	
	Observed	Calculated[a]
Methyl ^{13}C	47.7–48	47.3
Ortho ^{13}C	46–47	48.6
Meta ^{13}C	3.8–4.6	2.74
Para ^{13}C	1.0–1.1	1.37
1-Position ^{13}C	0–0.6	0
Ring/methyl	1.09	1.11

[a] Calculated from an equilibrated mixture of conjugated (94.5%) and nonconjugated (4.5%) heptatrienes according to the pathways described in Scheme 6.

Steric repulsion between such terminal methyl and methylene groups in species (d_2) precludes planar configurations, inhibits π-orbital overlap, and prevents thermal cyclization. Consequently, isomerization of (d) to species (e) or (f) must preceed cyclization; therefore, the equilibrium between the latter two species determines the relative contributions of conjugated and nonconjugated trienes to thermal cyclization pathways.

At 723 K, the equilibrium mixtures of *reactive* heptatrienes contain approximately 94.5% conjugated (1, *cis*-3, *trans*-5) and 5.5% nonconjugated (1, *cis*-3, 6) heptatrienes. Table 4 shows the excellent agreement between experimental toluene isotopomer distributions and those formed from such equilibrated heptatriene mixtures using the cyclization pathways described in Scheme 6. Experimental ring to methyl ^{13}C ratios (1.09) agree well with the value of 1.11 predicted by the heptatriene cyclization model. Dehydrocyclization occurs mostly by (1,6) ring closure, as expected from the higher stability of conjugated heptatrienes, and leads to predominant ^{13}C enrichment at ortho and methyl carbons in toluene. The slight ^{13}C enrichment observed at the 1-(ipso) position and the higher than predicted enrichment at the meta position (Table 4), especially at higher conversion, are consistent with a slight contribution of methyl shift isotopic isomerization of the predominant ortho-^{13}C species:

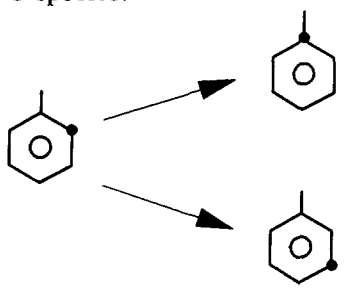

The proposal that heptatrienes are reactive intermediates is also consistent with our study of 3,3-dimethylhexane reactions on Te/Na*X* (723 K, 4.5 kPa hydrocarbon). The presence of a quaternary carbon in 3,3-dimethylhexane prevents triene formation but still allows the formation of olefin and diene intermediates. We have not observed the formation of dimethycyclohexane (ene) products on Te/Na*X*, in spite of their thermodynamic stability under these reaction conditions, even after achieving equilibrium levels of 3,3-dimethyhexene intermediates. It appears that the inability of 3,3-dimethylhexane to form triene species prevents cyclization events. Xylenes and ethylbenzene are formed from 3,3-dimethylhexane only after it isomerizes via bond shift to isoparaffins not containing a quaternary carbon. Therefore, alkane cyclization on Te/Na*X* must occur only after olefin, diene, *and* triene formation. In contrast, 3,3-dimethylhexane conversion to dimethylcyclohexane (ene) occurs readily on Pt catalysts, on which cyclization occurs by direct alkane chemisorption and ring closure without the requirement for unsaturated heptatriene intermediates (*40*).

5.2 Isomerization/Hydrogenolysis Pathways on Te/NaX

Isoparaffins formed from *n*-heptane-1-^{13}C show ^{13}C enrichment only at terminal carbon positions on Te/Na*X* (Table 3). Moreover, no *n*-heptane-4-^{13}C is observed in the reaction products (Scheme 2, Pathways B and C). These data, the low 3-methylhexane to 2-methylhexane ratios (~1) and ethylpentane selectivity (<1%) (Table 1) compared

to those expected from alkylcyclopentane hydrogenolysis, suggest that *n*-heptane isomerization does not involve C_5-ring intermediates on Te/Na*X*. Such intermediates are typical of alkane isomerization reactions on small metal particles and lead only to ethylpentane, 2,3-dimethylpentane, and 3-methylhexane isomers (*23*). On Te/Na*X*, isomerization requires olefin intermediates and proceeds via a bond-shift mechanism, probably on weak acid sites on Te/Na*X*. The absence of metal-catalyzed cyclic isomerization pathways further supports the lack of a catalytic cyclization function on Te/Na*X*; Te sites perform only a dehydrogenation function, and ring closure appears to occur exclusively by thermal cyclization of the resulting triene species.

Isomerization of 3,3-dimethylpentane also requires olefin intermediates and strongly favors 2,3-dimethylpentane, an initial product of methyl-shift pathways, over 2,2-dimethylpentane, a predominant product of isomerization via C_5-ring hydrogenolysis reactions.

Product intercept, contact time, and isotopic tracer studies are consistent with olefin intermediates in *n*-heptane isomerization. Intercept studies suggest that isomerization requires the presence of both Te and Na*X* components; no thermal isomerization was observed. The requirement for olefinic intermediates and the observed methyl shift pathways, characteristic of carbonium ion chemistry, suggest that isomerization reactions on Te/Na*X* are catalyzed by acid sites. Such acid sites, however, are not present in neat Na*X*, but only in Te/Na*X* catalysts. The generation of acid sites during Te deposition, the presence of a Te–Na*X* mixed site, or a polarization effect of surface Na^+ from cationic sites by Te may be responsible for such synergistic acid-type functionality.

Cracking products of *n*-heptane reactions on Te/Na*X* arise predominantly from thermal reactions, leading to C_2–C_6 olefin/paraffin ratios higher than thermodynamic predictions. Measured heptene thermal cracking rates were about fivefold higher than those of *n*-heptane, but the product distributions were identical. Thermal *n*-heptane reaction rates and C_1–C_6 distributions agree well with a model that assumes equilibrated heptyl radical distributions formed from *n*-heptane/heptane mixtures by healing of methyl and ethyl radicals (Scheme 4, chain propagation; Fig. 8) and uses previously reported rate constants (*32*). Thermal cracking rates are similar to those observed on Te/Na*X*. However, the primary cracking distribution is perturbed on Te/Na*X* by a secondary olefin dimerization reaction that predominantly converts ethylene products into C_4 and C_6 hydrocarbons.

Thermal cracking and olefin dimerization pathways account for C_1–C_6 products on Te/Na*X*. This suggests that neither acid nor metal functionalities contribute significantly to the measured rate of C_1–C_6 formation on Te/Na*X*.

CONCLUSIONS

Isotopic tracer studies suggest that dehydrocyclizaton occurs by sequential dehydrogenation of *n*-heptane to heptatrienes followed by gas-phase cyclization. Isotopomer distributions in toluene formed from *n*-heptane-1-^{13}C are consistent with a thermal electrocyclic addition reaction of an equilibrated mixture of conjugated and unconjugated heptatrienes. Sequential dehydrogenation rates on Te/Na*X* are limited by a hydrogen desorption elementary step that results in high hydrogen surface pressures. These hydrogen overpressures inhibit dehydrogenation rates by limiting the heptene, heptadiene, and heptatriene concentrations to values in equilibrium with virtual surface pressures rather than with gas-phase dihydrogen pressures.

In contrast with noble metal catalysts (e.g., Pt, Ir, Rh), Te/Na*X* appears to have no surface functionality for (1,6) or (1,5) ring closure or hydrogenolysis. Alkane isomerization occurs via a bond-shift mechanism involving olefin intermediates and resembling acid-catalyzed carbonium ion chemistry. C_1–C_6 products arise predominantly

from thermal cracking of alkanes, alkenes, and other noncyclic unsaturated intermediates. Thermal cracking product distributions are perturbed on Te/Na*X* by a catalytic dimerization of olefinic cracking products.

REFERENCES

1. Maile, J. N., and Weisz, P. B., *J. Catal.* **20,** 288 (1971).
2. Mikovsky, R. J., Silvestri, A. J., Dempsey, E., and Olson, D. H., *J. Catal.* **22,** 371 (1971).
3. Olson, D. H., Mikovsky, R. J., Shipman, G. F., and Dempsey, E. J., *J. Catal.* **24,** 161 (1972).
4. Lang, W. H., Mikovsky, R. J., and Silvestri, A. J., *J. Catal.* **20,** 293 (1971).
5. Silvestri, A. J., and Smith, R. L., *J. Catal.* **29,** 316 (1973).
6. Price, G. L., PhD dissertation, Rice University (1979).
7. Price, G. L., Ismagilov, Z. R., and Hightower, J. W., *in* "Proceedings, 7th International Congress on Catalysis, Tokyo, 1980" (T. Seiyama and K. Tanabe, Eds.), Part A, p. 708. Elsevier, Amsterdam/New York, 1981.
8. Price, G. L., Ismagilov, Z. R., and Hightower, J. W., *J. Catal.* **73,** 361 (1982).
9. Price, G. L., Ismagilov, Z. R., and Hightower, J. W., *J. Catal.* **81,** 369 (1983).
10. Price, G. L., and Egedy, G. R., *J. Catal.* **84,** 461 (1983).
11. Hightower, J. W., and Price, G. L. *ACS Symp. Ser.* **288,** 88 (1985).
12. Mitchell, J. J., *J. Amer. Chem. Soc.* **80,** 5848 (1958).
13. Chen, C. T., Haag, W. O., and Pines, H., *Chem. Ind.,* 1379 (1959).
14. Turner, H. S., and Warner, R. J., *Chem. Ind.,* 364 (1959).
15. Pines, H., and Goetschel, C. T., *J. Org. Chem.* **30,** 3530 (1965).
16. Feighan, J. A., and Davis, B. H., *J. Catal.* **4,** 594 (1965).
17. Derbentsev, Yu. I., and Isagulyants, G. V., *Russ. Chem. Rev.* **38**(9), 714 (1969).
18. Davis, B. H., and Venuto, P. B., *J. Org. Chem.* **36,** 337 (1971).
19. Haag, W.O., *Ann. N.Y. Acad. Sci.* **213,** 228 (1973).
20. Davis, B. H., *J. Catal.,* **29,** 398 (1973).
21. Amir-Ebrahimi, V., Choplin, A., Parayre, P., and Gault, F. G., *Nouv. J. Chim.* **4,** 431 (1980).
22. Nogueira, L., and Pines, H., *J. Catal.* **70,** 404 (1981).
23. Gault, F. G., *in* "Advances in Catalysis" (D. D. Eley, H. Pines, and P. B. Weisz, Eds.), Vol. 30, p. 1. Academic Press, New York (1981).

24*a*. Rozengart, M. I., Mortikov, E. S., and Kazansky, B. A., *Dokl. Akad. Nauvk SSSR* **158,** 911 (1964); **166,** 619 (1966).

24*b*. Kazansky, B. S., Isagulyants, G. V., Rozengart, M. I., Dubinsky, Yu. G., and Kovalenko, L. I., *in* "Proceedings, 5th International Congress on Catalysis, Palm Beach, 1972" (J. W. Hightower, Ed.), p. 1277. North-Holland, Amsterdam, 1973.

25*a*. Derbentsev, Yu. I., and Isagulyants, G. V., *Russ. Chem. Rev.* **38**(9), 714 (1969).

25*b*. Paal, Z., and Tetenyi, P., *Acta Chim. Acad. Sci.* Hung. **54,** 175 (1967); **55,** 273 (1968); **58,** 105 (1968).

26. Anderson, J. R., *in* "Advances in Catalysis" (D. D. Eley, H. Pines, and P. B. Weisz, Eds.), Vol. 23, p. 1. Academic Press, San Diego, 1973.
27. Anderson, J. R., and Avery, N. R., *J. Catal.* **5,** 446 (1966).
28. Anderson, J. R., and Macdonald, R. J., *J. Catal.* **19,** 227 (1970).
29. Anderson, J. R., Macdonald, R. J., and Shimoyana, Y., *J. Catal.* **20,** 147 (1971).
30. Pines, H., "The Chemistry of Catalytic Hydrocarbon Conversions." Academic Press, San Diego, 1981.
31. Appleby, W. G., Avery, W. H., and Meerbott, W. K., *J. Amer. Chem. Soc.* **69,** 2279 (1947).
32. (*a*) Tsang, W., *J. Phys. Chem. Ref. Data* **17**(2), 887 (1988); (*b*) Allara, D. L., and Shaw R., *J. Phys. Chem. Ref. Data* **9**(3), 523 (1980).
33. Vaughan, D. E. W., and Gosh, A. K., US Patent 4,832,824 (1989).
34. Iglesia, E., and Baumgartner, J., in preparation.
35. We were unable to obtain reliable thermodynamic data for 2- and 3-heptene isomers. As a result, we have measured equilibrium heptene/*n*-heptane ratio by reacting *n*-heptane on a Pt catalysts on which both ^{13}C tracer studies and hydrocarbon–deuterium exchange showed very rapid C and H equilibration between heptenes and *n*-heptane (500–773 K, 50–600 kPa dihydrogen pressure). The measured equilibrium heptene/*n*-heptane ratios under the conditions of this paper (723 K, 96 kPa dihydrogen) are: 0.0061 for 1-heptene, 0.016 for *cis*-2-heptene, and 0.027 for *trans*-2-heptene (as shown in Fig. 3).
36. Iglesia, E., and Baumgartner, J., submitted for publication.
37. Egger, K. W., and James, T. L., *Trans. Faraday Soc.* **66,** 410 (1970).
38. Egger, K. W., and Jola, M., *Int. J. Chem. Kinet.* **2,** 265 (1970).
39. Morrison, R. T., and Boyd, R. N., "Organic Chemistry," 3rd ed. Allyn and Bacon, Boston, 1973.
40. Iglesia, E., and Baumgartner, J., unpublished results.
41. Haag, W. O., and Pines, H., *J. Amer. Chem. Soc.* **82,** 2486 (1960).